Probing the Critical Region of Conductive Filament in Nanoscale HfO$_2$ Resistive-Switching Device by Random Telegraph Signals

Zheng Chai, Jigang Ma, Weidong Zhang, Bogdan Govoreanu, Jian Fu Zhang, Zhigang Ji, Malgorzata Jurczak

Abstract— **Resistive switching random access memory (RRAM) is widely considered as a disruptive technology. Despite tremendous efforts in theoretical modeling and physical analysis, details of how the conductive filament (CF) in metal-oxide based filamentary RRAM devices is modified during normal device operations remain speculative, because direct experimental evidence at defect level has been missing. In this work, a random-telegraph-signal (RTS) based defect tracking technique (RDT) is developed for probing the location and movements of individual defects and their statistical spatial and energy characteristics in the CF of state-of-the-art hafnium-oxide RRAM devices. For the first time, the critical filament region of the CF is experimentally identified, which is located near, but not at, the bottom electrode with a length of nanometer scale. We demonstrate with the RDT technique that the modification of this key constriction region by defect movements can be observed and correlated with switching operation conditions, providing insight to the resistive switching mechanism.**

Index Terms— **Resistive switching, conductive filament profiling, RRAM, random telegraph signal, hour-glass model, HfO$_2$.**

I. INTRODUCTION

Resistive switching random access memories (RRAM) are widely considered as a disruptive technology in digital memory, logic and neuromorphic computing [1-10]. Valence Change Memory (VCM) is an important category of such devices, in which it is believed that the resistive switching is controlled by the drift/diffusion of anions and/or cations, typically oxygen ion and/or its vacancy in a thin oxide dielectric layer, inducing local valence change in the atomic lattice [11]. For example, bipolar switching behavior has been reported in many oxides such as HfO$_2$, Ta$_2$O$_5$, Al$_2$O$_3$, TiO$_2$, SrTiO$_3$, etc. [4-5,11-12], where it is believed that a conductive filament (CF) throughout the oxide layer can be formed under a positive voltage, lowering the resistance of the device into a low resistive state (LRS). The CF can be ruptured by applying a negative voltage, returning to a high resistance state (HRS). It is therefore of critical importance to gain insight into the CF modification process, for example, the position of its constriction and how its profile is modified by the defects.

While promising results have been achieved by tremendous efforts in the past decade [4-5, 11-12], details of the underlying microscopic picture of the switching process are still largely missing. High-resolution physical analysis techniques have been used to probe the CF. 3-D tomography with conductive atomic force microscopy (scalpel-SPM) provides a 3D image of the conductive filament of a HfO$_2$ device at LRS [13,14] but does not have the required sensitivity to probe the CF at HRS due to the

reduced conductivity. Scanning tunneling microscopy (STM) provides the ultimate lateral resolution, but is limited to probing the surface of bare materials [17, 18]. *In situ* transmission electron microcopy (TEM) [15, 16] has linked sub-10 nm conductive channels to the local migration of oxygen vacancies, however, it is destructive, time consuming and statistically unfriendly. It is not clear how oxygen vacancies migrates under normal operating conditions, both individually and statistically, and hence it is not clear how it leads to the CF alteration between HRS and LRS.

Furthermore, due to lacking a clear picture of the CF at HRS, different CF profiles have been assumed in modelling and simulation, i.e., either with a conical shape [3, 19] or an hour-glass shape [20], respectively, and the CF modification was attributed either to the oxygen vacancy and oxygen pair ($V_O^{\bullet\bullet}$-O_i'') generation/recombination at the interface of the bottom electrode [19] or to the $V_O^{\bullet\bullet}$ movements along the CF [20], causing confusions and controversies. Direct experimental evidence of CF modification at defect level is needed to provide insight to the CF rupture/restore process, to improve our understanding of the switching mechanism and to advance the filamentary RRAM technology. In this work, a random telegraph signal (RTS) based defect tracking technique (RDT) has been developed that can detect individual defect movement and provide statistical information of CF modification during normal operations of nanoscale RRAM devices, and for the first time, without device destruction.

II. DEVICES AND EXPERIMENTS

The RRAM device under investigation is a TiN/Hf/HfO$_2$/ TiN memory cell patterned into a crossbar shape [21]. The Hf/HfO$_2$ element is formed in the overlap region between the bottom and top TiN electrodes, achieving 40nm×40nm cell size. The 5-nm thick HfO$_2$ dielectric, deposited by atomic layer deposition (ALD) is mainly amorphous. On top of the HfO$_2$ film, a 10-nm thick Hf metal-cap was deposited by physical vapor deposition (PVD) acting as an oxygen reservoir during the device operations. After an initial electroforming process to form the HfO$_{2-x}$ filament, typical current-voltage characteristics show a stable bipolar resistive-switching behavior: set to a low resistance state (LRS) at less than 1 V, and reset to a high resistance state (HRS) at about -1 V as shown in Fig.1a. The maximum current flowing through the device during the set is limited at a predefined compliance current, Icc, between 50 μA and 150 μA to avoid breakdown.

In order to investigate the defects that result in the CF without destructing the device, we use the random telegraph signals (RTS) as the electrical measurement tool [22, 23]. The origin of RTS is attributed to the random electron trapping/detrapping process in a defect located in the oxide from/to the electrode, leading to the two discrete, high and low, current levels, as shown in Fig.1b. The mean time constants for high (τ_{high}) and low (τ_{low}) current levels in

RTS are the capture (τ_c) and emission times (τ_e), respectively, [23] for electron tunneling between an electrode and a trap, and their bias dependence is governed by [22]

$$\frac{\tau_c}{\tau_e} = e^{(E_T - E_F)/K_B T} \qquad (a)$$

where $K_B T$ is the thermal energy, E_F is the Fermi level of the TiN electrode. Trap energy level (E_T) can thus be directly extracted from the dependence of τ_c/τ_e on top electrode bias,

$$K_B T \cdot \ln\left(\frac{\tau_c}{\tau_e}\right) = \Phi_0 - \left[(E_{C,ox} - E_T) + \left| q \cdot \frac{X_T}{T_{OX,TCR}} \cdot V_{ox} \right| \right] \qquad (b)$$

where Φ_0 is the difference between the work function of TiN and electron affinity of HfO_{2-x}, and is set to 1.4 eV [24]. $E_{C,ox}$ is the conduction band edge of the HfO_{2-x}, $T_{ox, TCR}$ is the thickness of the tunneling conduction region (TCR) in HfO_2, X_T is the trap location within TCR, and V_{ox} is the voltage drop over the TCR. $X_T/T_{OX,TCR}$ can be derived by differentiating (b) vs V_{ox},

$$\frac{X_T}{T_{OX,TCR}} = \frac{K_B T}{q} \cdot \frac{\partial}{\partial V}\left[\ln\left(\frac{\tau_c}{\tau_e}\right) \right] \qquad (c)$$

Fewer efforts have been made to investigate the RTS in RRAM because complex signals are often observed [24-25], to which the above equations are often not applicable. For example, defect movement and electron trapping/ detrapping can co-exist [25], both of which can result in current fluctuation and lead to complex signals. Moreover, Equations (a)-(c) are only applicable to the cases that an electron tunnels from an electrode to an oxide defect, and then back to the same electrode, in which τ_c and τ_e should have the opposite polarity of bias dependence. However, due to the nanoscale oxide thickness in RRAM devices, RTS can also result
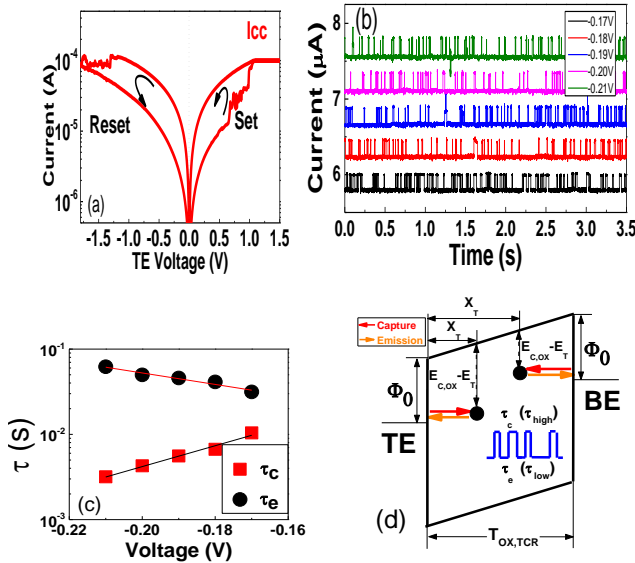

Fig. 1 (a) The bipolar resistive switching characteristics of a 40 nm HfO_2 memory cell. (b) Typical RTS signals under various TE biases. (c) The mean capture and emission time constants (τ_c and τ_e) measured during the voltage sweep, from which defect's spatial and energy location (X_T, E_T) is extracted with Eqs. (a)-(c). (d) Energy band diagram illustrating RTS caused by electron capture and emission. TE Bias is incremented during RTS measurement from ±0.1V to ±0.35V, V_{step} =±0.01V, time=3.5s/step. R is measured at 0.1V. Charging/discharging from both TE or BE are considered in this work. Defect distance to BE is converted to its distance to TE when the defect interacts with BE.
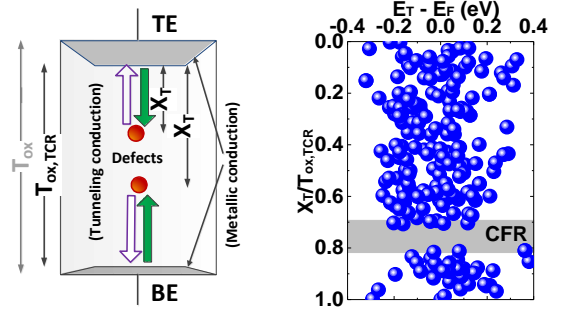

Fig. 2 (a) Illustration of the metallic conduction region near both electrodes, in which Equations (a)-(c) are not applicable. Defect's relative location within the electron tunnelling conduction region TCR, X_T/T_{ox_TCR}, can be extracted from Eq. (c) even though the absolute value of $T_{ox,TCR}$ is unknown. (b) Defects detected at HRS during DC switching cycles clearly show the CFR (grey region) with the least number of defects near, but not at, the BE. DC Vset=1V, Vreset= -1.6V, Icc=150uA.

from electron tunneling through the defect to the opposite electrode or to other defects, in which cases τ_c and τ_e show the same polarity of bias dependence. There also might be a large quantity of defects near each electrode, which leads to metallic-like local conduction. To avoid these complications, in this work, we only consider RTS that clearly follows the classical theory, as shown in Fig. 1. All RTS signals are evaluated individually and we only use signals for which τ_c and τ_e have the opposite polarity of bias dependence. This ensures that the defects we examined are located in the electron tunneling region of the oxide, and the RTS caused by electrons tunneling through the defects are excluded. We also use $X_T/T_{ox,TCR}$ as the defect's relative spatial location within the electron tunneling conduction region, TCR, as shown in Fig.1d & Fig.2a, thus avoiding the uncertainties brought by the metallic-like local conduction regions near the metal electrodes. We will show in the following that clear correlations between RTS, defect and filament are revealed by using the technique we developed in this work after taking the above factors into account.

III. RESULTS AND DISCUSSIONS

A. Observation of the critical filament region

The first key observation in this work, the critical filament region (CFR) in the TCR, was achieved by statistically analyzing the defect spatial location and energy level during normal device operation cycles. The switching behavior of filamentary RRAM devices has been described by various controversial models. The analytical hour-glass model [20] describes the CF as an hour-glass shaped sub-stoichiometric HfO_{2-x} region and the switching between LRS and HRS is determined by the changes in the number of $V_O^{\bullet\bullet}$ in its constriction. On the other hand, other Monte Carlo simulations and physics-based HSpice compact models [3, 19] assumed a conical-shaped CF, which is ruptured from the electrode during reset and is restored back to the same electrode during set, and the mechanism was attributed to $V_O^{\bullet\bullet}$-O_i'' pair generation and recombination as in ref. [19].

In order to help clarify this controversy, in this work, we switched the devices repeatedly between the LRS and HRS for a number of cycles, during each cycle the RTS measurement was

carried out at HRS to extract the defects locations. A large number of defect occurrences can therefore be collected during the cycling operation. A summary of the measured defects profile at HRS is shown in Fig. 2b, and a region (grey) with the least defect occurrences near, but not at, the BE can be clearly observed. This is the first time that the critical filament region is experimentally observed entirely based on the analysis of electrical data, The large number of defect occurrences observed nearby the BE does not support the conical model, which assumes that at HRS the filament is ruptured from the interface of the electrode where the least defects should occur. The CFR is not located in the center of the TCR either, which is a consequence of asymmetric oxygen vacancy reservoirs. Since the 10 nm Hf metal layer is intentionally inserted at the TE interface as the oxygen reservoir to increase the $V_O^{\bullet\bullet}$ concentration in HfO_2 near TE, it is therefore understandable that the CFR is located near BE, agreeing with the results of hour-glass modeling [20, 25].

B. Verification of CFR by defect movement tracking

Since the critical filament region has the least occurrences of defects and hence the largest local resistance, the movement of defects into and out of the constriction should have the most significant impact on CF resistance, leading to CF modification and resistive switching. To verify this, we further developed the RTS technique to enable the tracking of individual defect movements and the defect drift-diffusion process in the HfO_{2-x} to be correlated directly with CF modification and switching.

Fig.3a shows an example of the typical defect-tracking test results. During the bias increments of the RTS measurement at HRS, current jumps, either upwards or downwards, can be observed, which is associated with a simultaneous change in device resistance. In this particular example, the current jumps downwards during the bias sweeping, and the resistance measured at the read voltage of 0.1 V increases simultaneously, supporting

that the current jumps are caused by the modification of CF. The RTS and the bias dependence of the RTS time constants extracted before and after the current jumps also changes simultaneously as shown in the inset of Fig.3a and Fig.3b, resulting in a change of the extracted defect location, as shown in Fig.3c, i.e. defect moves out of the critical filament region as identified in Fig.3, leading to the CF modification and an increase of resistance.

To further verify the correlation between defect movement and CF modification, the relative change of the read current, $\Delta I/I$, are analyzed statistically against the defect locations before and after defect movements. Fig.4a shows that the increases of $\Delta I/I$ are correlated with defect moving into the highlighted CFR region (red rectangle), either from the TE direction or the BE direction, and the decreases of $\Delta I/I$ are correlated with defect moving out of the CFR region (blue rectangle), either towards the TE direction or the BE direction. The largest amplitudes of $\Delta I/I$ are clearly observed when the CFR region is either the destination or the origin of defect movements. These results highlight the importance of the start/stop location of defect movements. $\Delta I/I$ is small when defect movement is not involved with the CFR region, contributing less to switching. A broad correlation can also be obtained between the amplitude of $\Delta I/I$ and the relative distance of the defect movement regarding the constriction position, Xc, as shown in Fig. 4b. The farther away relatively from the constriction the movement is, the larger change in read current can be statistically observed. The above correlations provide strong statistical evidence supporting that our technique can indeed track defect movement, because it is impossible for two defects randomly detected in the oxides before/ after the jump to have such a correlation with resistance switching.

Further details of the defect movement mechanism can also be revealed by the defect movement dependence on the external bias
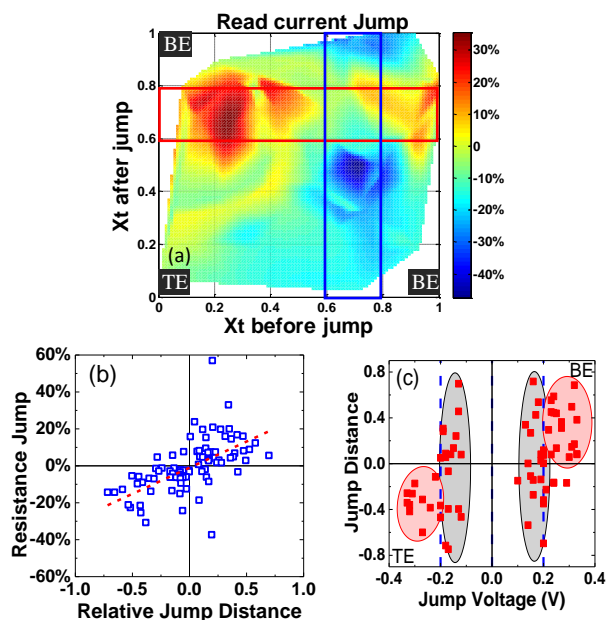
Fig.4 Correlation between defect movements and filament modification. a) Statistical analysis of the relative read current change $\Delta I/I$ vs X_T before and after defect movement. (b) Positive correlation between $\Delta R/R$ vs relative movement against constriction position Xc: $|X_{t,after}-Xc|-|X_{t,before}-Xc|$. (c) Defect moves towards BE ($\Delta X_T>0$) at V>0.2V, and moves towards TE ($\Delta X_T<0$) at V<-0.2V. Defect moves in either direction at -0.2V<V<0.2V.
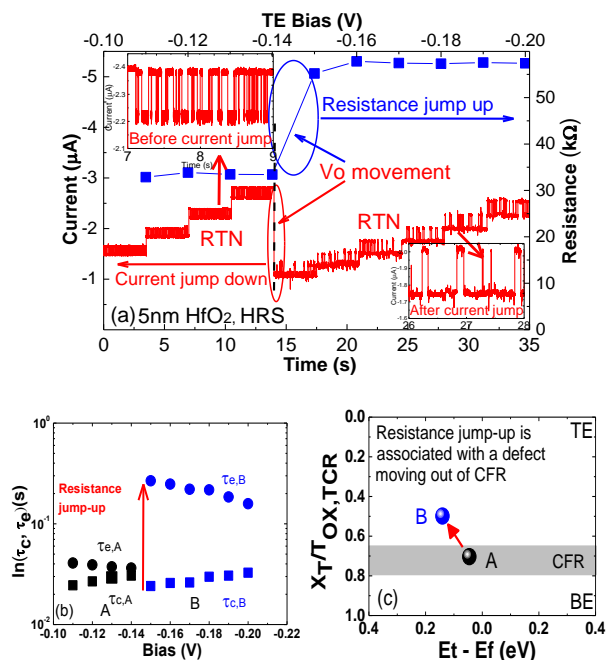

Fig.3 RTS based defect tracking (a) RTS signals consist of both defect movement and trapping-detrapping induced RTS. Measurement conditions are the same as in Fig. 1 & 2. (b) τ_c and τ_e measured before/after the R jump, from which (c) defect movement in (X_T , E_T) is extracted.
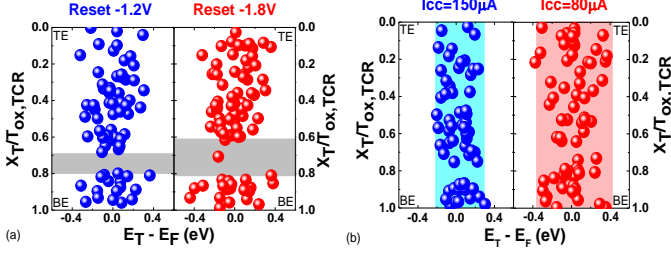
Fig.5 (a) Constriction is widened at a higher Vreset, and R at HRS increases from 12.5kΩ to 50 kΩ . Vset=1V. (b) Defects have a wider energy distribution at a lower compliance I_{CC}, probably due to weaker regulation during SET.

Fig.7 Distributions of (a) relative RTS amplitude $(\Delta I/I)_{RTN}$ and (b) absolute RTS amplitude ΔI_{RTS}, at LRS, weak LRS, and HRS. The distribution becomes wider at higher resistance and a significant tail at large RTS amplitude is observed for both relative and absolute RTS amplitude.

and its polarity. As shown in Fig. 4c, defect moves mainly towards BE at V>0.2V, and mainly towards TE at V<-0.2V, agreeing with that defects drift according to the direction of electric field at a large bias, underpinning the mechanism of the set/reset operations. At a weaker Eox when -0.2V<V<0.2V, which is often encountered during the read operation and write/read disturbance, defect can move in either directions, suggesting that defect movement is controlled by internal stochastic thermal/chemical processes. The above results indicate that the defect movement may be dominated by oxygen vacancy movements in O-deficient HfO_{2-x} with the scavenging Hf layer, as it is suggested that very little energy is required in such a structure [27, 28]. In contrast, interstitial O formation may require more than 6 eV to form the oxygen vacancy [28] which may be unlikely to be provided by a bias as small as 0.2 V.

C. Correlation of CFR modification with operation conditions

Further correlations between the modification of the CFR region at HRS and different operation conditions can be clearly observed by applying the RTS technique, for the first time. As shown in Fig. 5a, increasing Vreset from -1.2 V to -1.8 V widens the CFR mainly towards to the inner bulk of the oxide, thus increases the resistance at HRS from 12.5 kΩ to 50 kΩ. Reducing the maximum compliance current during the set operation, Icc, from 150 uA to 80 uA, as shown in Fig. 5b, widens the defect energy distribution probably due to the weaker regulation power caused by the lower set current, which requires further confirmation. In Fig. 6a, in order to observe the difference in the CFR between HRS and LRS, set operation is terminated at a lower voltage of 0.6 V to result in a partial set where electron tunneling in the CF still dominates. This is because switching to a full-scale LRS at high Vset will lead to a
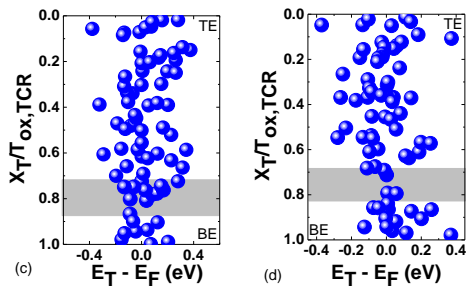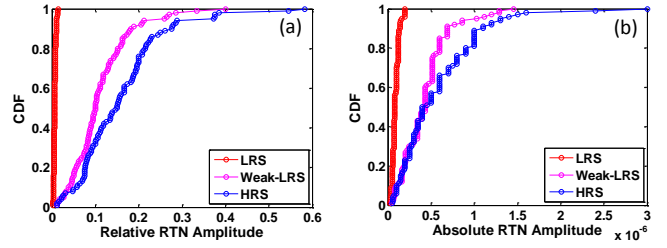
full metallic conduction path where the RTS technique is no longer applicable. More defects in the CFR can indeed be detected at the partial LRS, resulting in a weaker CFR and thus lower resistance. This result provides the experimental evidence of the difference in defect profiles at HRS and LRS, and reveals that the defect number in the CFR indeed determines the device resistance state. The CFR can also be observed in devices with the HfO_2 thickness scaled further down to 3 nm, as shown in Fig. 6b, confirming its applicability in devices further scaling into the lower nanometer regime.

Since the results demonstrate that the defect movements start to follow the direction of Eox at low electric field and lead to resistance change, it is therefore indicated that the positively charged oxygen vacancies are acting as the electron traps to produce the conductive path. During set operation from HRS towards LRS, the modification of the filament is initiated by the positive external electric field, which pushes defects towards the CFR mainly from TE direction. Thermal simulation confirmed our experimental results as temperature has a negligible role in the initiation of the HRS to LRS set process [29], especially at the low RTS measurement voltages. During the reset, defect movements from the CFR towards TE are dominant, resulting in a wider CFR and higher resistance. Our results also confirms that defects movement along the filament direction plays a dominant role in controlling the CFR modification, opposing to the cases of unipolar switching in which the defects move into and out of filament in the perpendicular direction in previous works [30]. Combined with previous results of physical characterization with c-AFM [14] and modeling [20] for the same devices, the results suggest that the filament has an hour-glass shape at HRS with the CFR located closer to the more oxygen-inert BE and the length of the constriction is less than 1 nm.

Fig.6 (a) At a partial LRS where electron tunnelling dominates, more defects can be detected within the CFR. Set: 0.6V, Reset: -1.4V, Icc=100 μA. (b) CFR is also observed near the BE in devices with 3nm HfO2 layer. Set: 0.65V, Reset: -1.4V, Icc=100 μA.

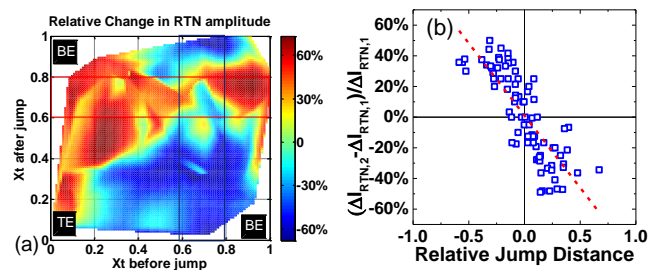Fig.8 Correlation between defect movements and relative RTN amplitude. (a) Statistical analysis of the change in relative RTN amplitudes $(\Delta I_{RTN,2}-\Delta I_{RTN,1})/\Delta I_{RTN,1}$ vs X_T before and after defect movement. (b) Negative correlation between $(\Delta I_{RTN,2}-\Delta I_{RTN,1})/\Delta I_{RTN,1}$ vs relative movement distance against the constriction position Xc: |Xt,after-Xc| - |Xt,before -Xc|.

Further evidence of the correlation between filament modification and the device operation can be obtained from the impact of defect movement on RTS amplitude. Fig. 7 compares the measured RTS amplitude distributions at HRS, weak LRS and LRS. The distribution becomes wider at higher resistance, and a significant tail is observed at large RTS amplitude, as compared to LRS, agreeing with previous results [26]. The large RTS amplitude at HRS suggests that the trapping/ detrapping into/from the defects within CFR may lead to large noise during device read operations. A statistical analysis of the RTS amplitude before and after the defect movements at HRS confirms this point. Fig.8a shows the increases of ΔI_{RTS} are correlated with $V_O^{\bullet\bullet}$ moving into the highlighted CFR region and the decreases of ΔI_{RTS} are correlated with $V_O^{\bullet\bullet}$ moving out of the CFR region. The largest changes in ΔI_{RTS} are clearly observed when the CFR region is either the destination or the origin of defect movements. These results are in agreement with the resistance change observed in Fig.4a. The change in ΔI_{RTS} is small when defect movement is not involved with the constriction. A broad correlation can also be obtained between the change in ΔI_{RTS} and the relative distance of the defect movement regarding the constriction position, Xc, as shown in Fig. 8b. The farther away relatively from the constriction the movement is, the larger change in ΔI_{RTS} can be statistically observed, agreeing with the observation in Fig.4b. A single charge trapping/detrapping in the CFR region may significantly alter a tunneling path and induce a large variation in tunneling current and thus a large RTS induced read noise. On the contrary, the CFR region is much less significant at LRS than at HRS, the impact of single trapping/detrapping becomes much weaker and thus RTS amplitudes are relatively small and much narrowly distributed.

D. Discussions

An overall picture of the switching mechanism in bipolar oxide-based RRAM has been provided in this work, showing the repeatable modification of the local critical filament region. The filament is formed by the generation of defects in the bulk of the oxide during electroforming, resulting in a percolation current path. Under the applied forming electric field, the oxygen ions drift toward the TE leaving behind the $V_O^{\bullet\bullet}$ forming a local conductive path in the HfO_{2-x}. The filament connects the top oxygen reservoir with the BE at LRS. During the resistive switching cycle the number of $V_O^{\bullet\bullet}$ in the CFR and the length of CFR, where it has the least defect occurrence and is closer to the bottom electrode, are changed by the defect movement according to the electric field at a bias as low as $\pm0.2V$, inducing the resistance change and eventually leading to the switching of resistance states.

It should be noted that the RTS method has its limitations. For example, the absolute location of defects, X_T, and their density distribution across the entire HfO_2 stack cannot be provided by this method. As a simplification approach, we use the relative defect depth, $X_T/T_{OX,TCR}$, in the tunneling conduction region (TCR), instead of the total thickness T_{OX}, to represent defect's location, and a uniform electric field distribution in the tunneling conduction region is also assumed, which has been commonly used in previous works [31-35]. We found that clear correlations among defect movements, defect profile, CFR modifications,

resistance changes, RTN amplitudes and the electrical programming conditions are revealed by using this technique despite these limitations. In addition, the dependence of defect movement direction on the bias polarity starting at a voltage as low as 200 mV is in agreement with the theoretical calculations and analysis in ref. [28], indicating, but not as a direct proof, that $V_O^{\bullet\bullet}$ movement is the responsible mechanism. The large number of defects occurrences observed near the bottom electrode is also in good agreement with the hour-glass shaped filament [20]. This demonstrates that although the real distribution in the TCR region may be, to certain level, non-uniform, but the level of non-uniformity may not be significant enough to affect the conclusions in this work. Further studies are required to reach unambiguous conclusions.

We would also like to emphasize that the RTS technique cannot provide the actual number or density of the defects in the filament. The profile observed in Fig. 2b is an accumulative plot of the defect occurrences detected at HRS during the cycling operation. It is not correlated to the actual defect number in the filament. When there is no defect observed in the critical filament region, it means that no defect occurrence has been detected for the duration of the test, while there are defects being detected in other regions. Less defect occurrence detected in the CFR indicates a smaller probability for defects to exist there. The analysis in the manuscript is based on defect occurrence, instead of the actual defect count or density.

The $V_O^{\bullet\bullet}$ assisted conduction current at HRS could be modulated either by the charging/discharging of an electron to/from a nearby neutral trap [35], or to/from the deeper states of $V_O^{\bullet\bullet}$ [36] and thus leading to RTS fluctuations with time constants larger than those through the shallow states of $V_O^{\bullet\bullet}$ that form the conduction current. This uncertainty, however, does not affect the analysis and conclusions in this work. The RTS provides the information of defect locations in both cases, and allows us to track defect movements and extract the defect profile.

Regarding the impact of defects at different locations, an electron could tunnel through the shallow states of several defects along a critical path across the TCR, instead of through only one defect in the narrowest critical filament region (CFR), to form the conduction current. It is likely that the defect number, being the least in the critical filament region, increases gradually towards both ends of the TCR, instead of changing abruptly from a constant low value in CFR (for TAT) to a very high value (for metallic conduction) immediately at the edge of CFR. A defect moved from position A to B may lead to different contributions to the conduction, depending on its relative distance and alignment to the CFR, as shown in Fig. 4b and Fig. 8b. The name of "critical filament region" (CFR), instead of the constriction, is used in this work, because it is possible that either the TCR or the CFR has more resemblance to the term "constriction" defined in other works. Further work is required to clarify this point.

After taking the above analysis into consideration, our RTS based filament characterization technique provides the physical insights of oxide based filamentary RRAM, improves the understanding of the filament and its critical region at defect level, and thus provides a useful tool for RRAM technology development.

IV. CONCLUSIONS

An RTS based technique has been developed in this work, which can monitor the defect location, movement and filament change during RRAM operations. Using this specifically designed RTS technique, for the first time, we have directly observed the critical filament region at HRS and at partial LRS in nanoscale devices that play the critical role in determining the resistive switching. We have established the correlation between the filament structure modifications and the electrical programming conditions, revealing the nature of resistive switching being controlled by modification of the critical filament region. The RTS technique can also track the individual defect movements, and provide its electric field dependence that controls the defect drift. Statistical analysis on the experimental results are enabled by the RTS technique, which demonstrates that defects moving into or out of the critical filament region is closely correlated with the resistance change and RTS amplitude, providing direct experimental evidence for the nature of resistive switching as defects modulating the CFR and its correlation with device operation conditions.

REFERENCES

[1] L. O. Chua, "Memristor-The missing circuit element", IEEE Trans. Circuit Theory, Vol. 18, No. 5, pp.507-519, 1971.

[2] R. Waser, M. Aono, "Nanoionics-based resistive switching memories", Nat. Mater. Vol. 6, No. 11, pp. 833 – 840, 2007.

[3] D. B.Strukov, G. S. Snider, D. R. Stewart, R. S. Williams, "The missing memristor found", Nature, Vol. 453, pp. 80-83, May, 2008.

[4] H. S. P. Wong, H.-Y. Lee, S. Yu, Y.-S. Chen, Y. Wu,; P.-S. Chen, B. Lee, F. T. Chen, and M.J. Tsai, "Metal-oxide RRAM", IEEE Proc., Vol. 100, No. 6, pp.1951-1970, 2012.

[5] D. S. Jeong, R. Thomas, R. S. Katiyar, J. F. Scott, H. Kohlstedt, A. Petraru, and C. S. Hwang, "Emerging memories: resistive switching mechanisms and current status," Rep. Prog. Phys. vol. 75, 076502, pp.1-31, June, 2012.

[6] I. G. Bae., M. S. Lee, S. Seo, M. J. Lee, D. H. Seo, D.-S. Suh, J.C. Park, S.O. Park, H.S. Kim, I.K. Yoo, U.-In. Chung, J. T. Moon, "Highly scalable nonvolatile resistive memory using simple binary oxide driven by asymmetric unipolar voltage pulses", IEDM, pp.587-590, Dec., 2004.

[7] J. Borghetti, G. S. Snider, P. J. Kuekes, J. J. Yang, D. R. Stewart, and R. S. Williams, "Memristive'switches enable 'stateful'logic operations via material implication", Nature, Vol. 464, pp.873-876, April, 2010.

[8] J. Cong, B. Xiao, "FPGA-RPI: A Novel FPGA Architecture With RRAM-Based Programmable Interconnects", IEEE Trans. VLSI Syst., Vol. 22 No. 4, pp.864-877, 2014.

[9] M. D. Pickett, G. Medeiros-Ribeiro, and R. S. Williams, "A scalable neuristor built with Mott memristors", Nat. Mater., Vol. 12, pp.114-117, Dec. 2013.

[10] G. W. Burr, R. M. Shelby, S. Sidler, C. di Nolfo, J. Jang, I. Boybat, R. S. Shenoy, P. Narayanan, K.Virwani; E U. Giacometti; B. N. Kurdi; and H. Hwang, "Experimental Demonstration and Tolerancing of a Large-Scale Neural Network (165000 Synapses) Using Phase-Change Memory as the Synaptic Weight Element", IEEE Trans. Elect. Dev, Vol. 62, No.11, pp.3498-3507, 2015.

[11] R. Waser; R. Dittmann; G. Staikov; K. Szot, "Redox-Based Resistive Switching Memories – Nanoionic Mechanisms, Prospects, and Challenges", Adv. Mater., Vol. 21, pp.2632-2663, Jul., 2009.

[12] J. S. Lee; S. Lee; T. W. Noh, "Resistive switching phenomena: A review of statistical physics approaches", Appl. Phys. Rew., Vol. 2, No. 3, 031303, 2015.

[13] U. Celano; L Goux et al. "Three-Dimensional Observation of the Conductive Filament in Nanoscaled Resistive Memory Devices", Nano Letts, Vol. 14, No. 5, pp.2401-2406, 2014.

[14] U. Celano; L. Goux; R. Degraeve; et al, "Imaging the Three-Dimensional Conductive Channel in Filamentary-Based Oxide Resistive Switching Memory", Nano Letts, Vol. 15, No. 12, pp.7970-7975, 2015.

[15] F. Miao,; J. P. Strachan,; J. J. Yang; Zhang, M. X. Zhang, I. Goldfarb, A. C. Torrezan, P. Eschbach, R. D. Kelley, G. Medeiros-Ribeiro, R. S. Williams, "Anatomy of a Nanoscale Conduction Channel Reveals the Mechanism of a High-Performance Memristor", Adv. Mater. Vol.23, pp.5633-5640, Nov. 2011.

[16] G.-S. Park; Y. B. Kim, S. Y. Park, X. S. Li, S. Heo, M. J. Lee, M. Chang, J. H. Kwon, M. Kim, U. I. Chung, R. Dittmann, R. Waser, K. Kim, "In situ observation of filamentary conducting channels in an asymmetric $Ta_2O5-x/TaO2-x$ bilayer structure", Nat. Commun., Vol. 4, pp.2382-2390, 2013.

[17] A. Nayak,; T. Tamura,; T. Tsuruoka,; K. Terabe,; S. Hosaka,; T. Hasegawa,; M. J. Aono, "Rate-Limiting Processes Determining the Switching Time in a Ag2S Atomic Switch", Phys. Chem. Lett. Vol. 1, No. 3, pp. 604−608, 2010.

[18] M. Moors, K. K. Adepalli, Q. Lu, A. Wedig, C. Bäumer, K.Skaja, B.Arndt, H. L. Tuller, R. Dittmann, R. Waser, B. Yildiz, and I. Valov, "Resistive Switching Mechanisms on TaOx and SrRuO3 Thin-Film Surfaces Probed by Scanning Tunneling Microscopy", ACS Nano, vol. 10, No. 1, pp.1481−1492, 2016.

[19] J. F. Kang, B. Gao, P. Huang, H. T. Li, Y. D. Zhao, Z. Chen, C. Liu, L. F. Liu, and X. Y. Liu, "Oxide-based RRAM: Requirements and challenges of modeling and simulation", IEDM, pp. 113-116, Dec. 2015.

[20] R. Degraeve, A. Fantini, S. Clima, B. Govoreanu, L. Goux, Y.Y. Chen, D.J. Wouters, Ph. Roussel, G.S. Kar, G. Pourtois, S. Cosemans, J.A. Kittl, G. Groeseneken, M. Jurczak, L. Altimime, "Dynamic 'hour glass' model for SET and RESET in HfO2 RRAM", Symp. VLSI Tech., pp.75-76, June, 2012.

[21] B. Govoreanu; G. S. Kar; Y-Y.Chen, V.Paraschiv, S. Kubicek, A.Fantini, I.P.Radu, L.Goux, S.Clima, R.Degraeve, N.Jossart, O.Richard, T.Vandeweyer, K.Seo, P.Hendrickx, G. Pourtois, H.Bender, L.Altimime, D.J.Wouters, J.A.Kittl, M.Jurczak, "10×10nm^2 Hf/HfOx crossbar resistive RAM with excellent performance, reliability and low-energy operation", IEDM, pp. 729-732, Dec. 2011.

[22] M. J. Kirton, M. Uren, "Noise in solid-state microstructures: A new perspective on individual defects, interface states and low-frequency ($1/f$) noise", Advances in Physics, Vol. 38, pp. 367-468, June, 1989.

[23] C. M. Chang; S. S. Chung, Y. S. Hsieh, L. W. Cheng, C. T. Tsai, G. H. Ma, S. C. Chien, and S. W. Sun, "The observation of trapping and detrapping effects in high-k gate dielectric MOSFETs by a new gate current Random Telegraph Noise (IG-RTN) approach", IEDM,, pp.787-790. Dec. 2008.

[24] S. Ambrogio; S. Balatti; A. Cubeta1; A. Calderoni; N. Ramaswamy; D. Ielmini, "Understanding switching variability and random telegraph noise in resistive RAM", IEDM, pp.782-785, Dec. 2013.

[25] N. Raghavan; R. Degraeve; L. Goux; A. Fantini; D. J. Wouters, G. Groeseneken and M. Jurczak, "RTN insight to filamentary instability and disturb immunity in ultra-low power switching HfOx and AlOx RRAM", Symp. VLSI Tech., pp.164-165, June, 2013

[26] Y. T. Chung, Y. H. Liu, P. C. Su, Y. H. Cheng, and T. Wang, "Investigation of random telegraph noise amplitudes in hafnium oxide resistive memory devices", IRPS, pp2.1-2.5, June, 2014.

[27] F. A. Kroger; H. J. Vink, "Relations between the concentrations of imperfections in solids", J. Phys. Chem. Solids Vol. 5, No.3, pp.208-223, 1958.

[28] Y.Guo and J. Robertson, "Materials selection for oxide-based resistive random access memories", Applied Phys. Lett., Vol., 105, 223516, 2014.

[29] B. Govoreanu; S. Clima; I. P. Radu; Y-Y Chen,D. J. Wouters, and M. Jurczak " Complementary role of field and temperature in triggering On/Off switching mechanisms Hf/HfO$_2$ Resistive RAM Cells", IEEE Trans. Elect. Dev, Vol. 60, No. 8, pp.2471-2478, 2013.

[30] D. B. Strukov, F. Alibart, and R. S. Williams, "Thermophoresis/diffusion as a plausible mechanism for unipolar resistive switching in metal–oxide–metal memristors", Appl. Phys. A: Mater. Sci. Process., Vol. 107, No.3, pp. 509-518, 2012.

[31] Jung-Kyu Lee, Ju-Wan Lee, Jinwon Park, Sung-Woong Chung, Jae Sung Roh, Sung-Joo Hong, Il-whan Cho, Hyuck-In Kwon, and Jong-Ho Lee, Extraction of trap location and energy from random telegraph noise in amorphous TiOx resistance random access memories, APPLIED PHYSICS LETTERS 98, 143502, 2011

[32] Y. J. Huang, Steve S. Chung, H. Y. Lee, Y. S. Chen, F. T. Chen, P. Y. Gu, and M. -J. Tsai, The Physical Insights Into an Abnormal Erratic Behavior in the Resistance Random Access Memory, IRPS, 2013

[33] Yuan Heng Tseng, Wen Chao Shen, Chia-En Huang, Chrong Jung Lin, Ya-Chin King, Electron Trapping Effect on the Switching Behaviour of Contact RRAM Devices through Random Telegraph Noise Analysis, IEDM, 2010

[34] Yuan Heng Tseng, Wen Chao Shen, and Chrong Jung Lin, Modeling of electron conduction in contact resistive random access memory devices as random telegraph noise, JOURNAL OF APPLIED PHYSICS 111, 073701, 2012,

[35] F. M. Puglisi, L. Larcher, A. Padovani, and P. Pavan "A complete statistical investigation of RTN in HfO2-based RRAM in high resistive state," IEEE Trans. Electron Devices, vol. 62, no. 8, pp. 2606-2613, Aug. 2015

[36] T. Grasser, "Stochastic charge trapping in oxides: From random telegraph noise to bias temperature instabilities", Microelectronics Reliability 52, pp.39–70, 2012.